Theor Chem Acc (2011) 130:1043–1053
DOI 10.1007/s00214-011-1059-9

REGULAR ARTICLE

Quantum chemical studies of Lindqvist-type polyoxometalates containing late 3d transition metals ($[(py)M^{II}W_5O_{18}]^{4-}$ (M = Fe, Co, Ni)): M^{II}–N bonding and second-order nonlinear optical properties

Sha Cong · Li Kai Yan · Shi Zheng Wen · Wei Guan · Zhong Min Su

Received: 28 April 2011 / Accepted: 26 September 2011 / Published online: 18 October 2011

Abstract The electronic and nonlinear optical (NLO) properties of Lindqvist-type tungstate containing late 3d transition metals $[(py)MW_5O_{18}]^{4-}$ (M = Fe, Co, Ni) have been systematically investigated using density functional theory (DFT) method. The character of M–N bond is analyzed using natural bond orbital methods. The first hyperpolarizabilities of $[(py)MW_5O_{18}]^{4-}$ anions have been investigated by Coulomb-attenuating method (CAM-B3LYP). The NLO properties of $[(py)MW_5O_{18}]^{4-}$ with different spin states are also studied. The results show that the static second-order polarizability (β_0) of $[(py)^5FeW_5O_{18}]^{4-}$ (Fe = quintet state) is 525.10×10^{-30} esu, which is larger than those of $[(py)^4CoW_5O_{18}]^{4-}$ ($\beta_0 = 120.72 \times 10^{-30}$ esu) and $[(py)^3NiW_5O_{18}]^{4-}$ ($\beta_0 = 30.45 \times 10^{-30}$ esu) anions. Time-dependent DFT results reveal that the substituted transition metals-to-pyridine charge transfer may be responsible for the NLO properties of this kind of polyoxometalates.

Keywords Polyoxometalates · Late 3d transition metals · Second-order polarizability · Density functional theory (DFT)

1 Introduction

Polyoxometalates (POMs) are a rich class of inorganic cluster [1–3] systems which are usually formed by W, Mo, or V. They exhibit remarkable chemical and physical properties which have been applied in a variety of fields ranging from medicine to nanotechnology [4–7]. The wide interest in the numerous important applications based on the properties of the molybdenum (Mo), tungstum (W), and vanadium (V) based POM cluster systems leads one to naturally investigate the properties of other metal (iron (Fe), Cobalt (Co), and nickel (Ni)) based POM cluster systems. During the past decade, there has been increasing interest in the functional group chemistry of POMs with organic derivatives [8]. The delocalized electrons coexist in both the organic networks and the inorganic clusters in organic–inorganic hybrid POMs. Therefore, one of the current issues of focus has been to make multifunctional hybrid materials using covalently linked POMs and organic polymers. Many organic–inorganic hybrids POMs have been reported [9, 10]. Among the organic derivatives of POMs, the derivatives of Lindqvist-type POMs have been continuously synthesized by Proust [11], Wei [12], Peng [13] and others [3, 14, 15]. Heterometallic Lindqvist-type anions are an important group in the organic–inorganic hybrids of Lindqvist-type. In recent years a lot of organic derivatives of heterometallic Lindqvist-type POMs were synthesized [16–19]. Most work concentrates on $[M_nW_{6-n}O_{19}]^{(2+n)-}$ and $[M_nMo_{6-n}O_{19}]^{(2+n)-}$ (M = Nb, V, Ti, and other early transition metals, n = 1–4) polyanions. Few derivatives of Lindqvist-type POMs with

Dedicated to Professor Akira Imamura on the occasion of his 77th birthday and published as part of the Imamura Festschrift Issue.

Electronic supplementary material The online version of this article (doi:10.1007/s00214-011-1059-9) contains supplementary material, which is available to authorized users.

S. Cong · L. K. Yan (✉) · S. Z. Wen · W. Guan · Z. M. Su (✉)
Department of Chemistry, Northeast Normal University, Institute of Functional Material Chemistry, Changchun 130024, People's Republic of China
e-mail: yanlk924@nenu.edu.cn

Z. M. Su
e-mail: zmsu@nenu.edu.cn

the molybdenum or tungsten atoms replaced by late transition metals have been reported. Recently, Errington et al. [20] have adopted a stepwise strategy involving the initial generation of the lacunary anion $[W_5O_{18}]^{6-}$ and its subsequent reaction with a Co^{II} salt to synthesize two CoW_5 heterometalates ($[\{CoW_5O_{18}H\}_2]^{6-}$ and $[(py)CoW_5O_{18}H]^{3-}$). $[\{CoW_5O_{18}H\}_2]^{6-}$ dissolved in pyridine gives a dark pink solution of the monomeric pyridine adduct $[(py)CoW_5O_{18}H]^{3-}$. The author also presented evidence for the formation of an analogous FeW_5 species [20].

Nonlinear optical processes are being increasingly exploited in potential applications in a variety of optoelectronic and photonic devices [21]. A significant amount of work has been done on electron-optical materials with different conventional strategies to enhance the NLO response. There exist three generic classes of NLO material: semiconductors, inorganic salts, and organic compounds. Each class possesses its own complement of favorable and unfavorable attributes for NLO applications [22]. Among these three kinds of NLO materials, the organic materials are of major interest because of their relatively low cost, ease of fabrication and integration into devices, tailorability that allows one to fine-tune the chemical structure and properties for a given nonlinear optical process, high laser damage thresholds, low dielectric constants, fast nonlinear optical response times, and off-resonance nonlinear optical susceptibilities comparable to or exceeding those of ferroelectric inorganic crystals [23]. Though organic materials have some advantages, they also have several disadvantages: low energy transitions in the UV–vis region enhance the NLO efficiency but result in a tradeoff between nonlinear efficiency and optical transparency, they may have low thermal stability, and undergo a facile relaxation to random orientation (in poled guest–host systems) [24]. So the new materials should be investigated to resolve the above problems.

POMs are excellent electron acceptors and can form electron donor–acceptor compounds [25, 26], so they have become new promising NLO materials. Over the past few years, considerable efforts have been directed toward the nitride or organoimido functionalization of redox-active closed-framework POMs [27] which are very useful for NLO materials. NLO properties of organoimido derivatives of hexamolybdates have been investigated by our group [28, 29] using density functional theory (DFT) formalism, which has been proved as a useful tool to investigate the properties of POMs [29–31]. From our previous work, we conclude that the formation of the Mo≡N triple bond increases delocalization of the aromatic π electrons and strong electronic interaction between the hexamolybdates and the organoimido moiety [32]. Lengthening of organoimido π-conjugation or increasing the organoimido polyanion can be used to increase the β or γ values. In Fig. 1 one can see the models of D-A-type polyoxometalates. One can see that the main electron transfer occurs from the organoimido(s) to the hexamolybdates (See Fig. 1a). In the present paper, we performed the quantum chemical calculations on $[(py)MW_5O_{18}]^{4-}$ ($M = Fe^{II}$, Co^{II}, and Ni^{II}) and elucidated the role of the pyridine and late transition metals in defining the bonding, electronic and NLO properties. The charge transfer character of $[(py)MW_5O_{18}]^{4-}$ will also be discussed.

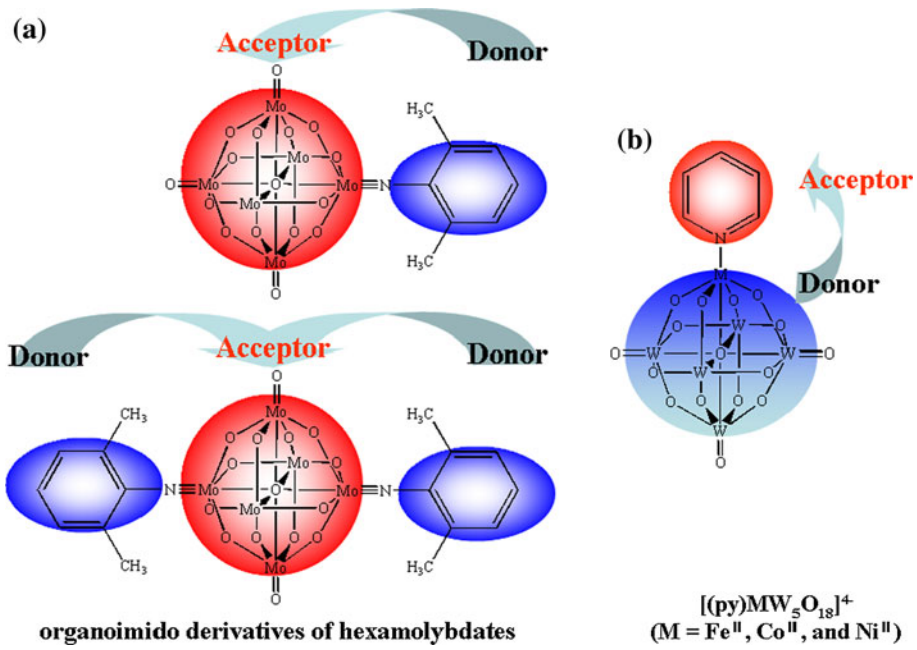

Fig. 1 Sketch map of D-A-type polyoxometalates

2 Computational details

2.1 Geometry optimization

The geometrical optimizations of all anions studied here were carried out using ADF 2008 program [33–35]. The zero-order regular approximation (ZORA) was adopted in the calculations to account for the scalar relativistic effects [36–39]. The generalized-gradient approximation (GGA) was employed in geometrical optimizations by using the Beck and Perdew (BP86) [40, 41] exchange–correlation (XC) functional, and VWN local density functional [42]. The triple-ζ basis plus polarization Slater-type orbital basis sets were used to describe the main group elements (O, C, N, and H), whereas for transition metal Fe, Co, and Ni atoms, a frozen core composed of 1*s* to 2*p* shells and for W atoms 1*s* to 4*d* shells were used. The value of the numerical integration parameter used to determine the precision of numerical integrals was 6.0 [31, 43]. The computational description of molecules in vacuum or in the gas phase has reached a remarkable state over the past years. But since nearly all technical chemistry does take place in the condensed phase, mainly in fluids, the proper theoretical and computational handling of molecules in solution and the proper calculation and prediction of the behavior and the thermodynamic properties of solute–solvent systems is very important for computational chemistry. To reduce the discrepancy between the gas-phase calculation and the solution phase measurement, the solvent effects were employed in the calculations of geometrical optimization and excitation properties by using the conductor-like screening model (COSMO) [44–47]. The solvent cavity surrounding the anion was created using the solvent-excluding method with fine tesserae. The solute dielectric constant was set to 4.34 (diethyl ether). The van der Waals radii for the POM and organic ligand atoms, which actually define the cavity in the COSMO, were chosen to be 1.49, 1.41, 1.40, 1.08, 2.10, 1.94, 1.92, and 1.84 Å for C, N, O, H, W, Fe, Co, and Ni, respectively [48]. Methods are necessary to be able to understand not only the interactions responsible for structural stability, but also to determine and understand their function [49–51]. In some calculations, the first salvation shell of solvent molecules are treated explicitly, rather than to use one of the many continuum solvent model treatments [52–54]. Additionally, the Onsager [55] and the polarized continuum model (PCM) [56] are used to calculate expect COSMO. Owing to the COSMO in ADF allows easy extraction of the Hessian from the output files for off-line processing. So the geometrical optimizations are also used the PCM in Gaussian 09 package [57] with the CAM-B3LYP [58, 59]. The basis set LANL2DZ associated with pseudo-potential was used to describe W and Co atoms, and the 6-31G(d) was employed to describe C, N, O and H atoms. Spin-unrestricted calculations were performed for all of the open-shell systems in this work. Geometrical optimizations of all systems under C_{2v} symmetry constraint was carried out. Their structures are sketched in Fig. 2.

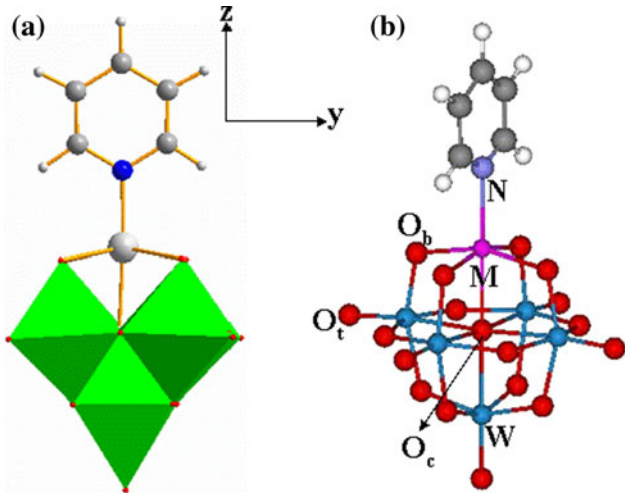

Fig. 2 Polyhedral and ball-and-stick representations of calculation model $[(py)MW_5O_{18}]^{4-}$ (M = Fe, Co, Ni)

2.2 NBO calculations

The chemical bonding between the metal-nitrogen bonds in each anion based on their optimized ground-state geometries was evaluated by NBO analysis of the density matrix obtained from UB3LYP single-point calculations. All NBO studies were carried out with the NBO 5.0 software package [60].

2.3 Second-order polarizability calculations

The first hyperpolarizabilities are evaluated by Finite Field (FF) approach with the CAM-B3LYP level using Gaussian 09 package. The basis set used for C, N, O and H atoms are the standard Gaussian basis set 6 − 31G(d), in which one set of d-polarization functions is included. For 5d transition metals, the basis set LANL2DZ was used. In FF method when a molecule is subjected to the static electric field (F), the energy (E) of the molecule is expressed by equation (1)

$$E = E^{(0)} - \mu_i F_i - \frac{1}{2}\alpha_{ij}F_jF_i - \frac{1}{6}\beta_{ijk}F_iF_jF_k - \frac{1}{24}\gamma_{ijkl}F_iF_jF_kF_l - \cdots, \quad (1)$$

where $E^{(0)}$ is the energy of molecule in the absence of an electronic field, μ is the component of the dipole moment vector, α is the linear polarizability tensor, β and γ are the first and second hyperpolarizability tensors whereas *i, j* and *k* label the *x, y,* and *z* components, respectively.

2.4 Excitation property calculations

Time-dependent density functional theory (TDDFT) is one of the most popular tools for studying the excitation properties in quantum chemistry due to its efficiency and accuracy. It has been used to investigate the electronic spectra of numerous systems, including closed- and open-shell systems [61–63]. By far, the accuracy and reliability of spin-unrestricted TDDFT methods for open-shell systems have been tested by organic and transition metal compounds [64, 65]. Herein, the statistical average of orbital potentials (SAOP) by Gritsenko, Baerends et al. [66] was used to calculate the excitation energies of $[(py)MW_5O_{18}]^{4-}$ (M = Fe^{II}, Co^{II}, and Ni^{II}).

3 Results and discussion

3.1 Geometrical structures

The Lindqvist-type heteropolyanion is made of six MO_6 octahedrons sharing their corners or edges. The oxygen atoms in the Lindqvist framework can be divided into three categories: central oxygen (O_c), bridge oxygen (O_b), and terminal oxygen (O_t). The structures of $[(py)MW_5O_{18}]^{4-}$ (M = Fe, Co, Ni) are sketched in Fig. 2.

Recently, Errington et al. [20] reported $[(py)CoW_5O_{18}H]^{3-}$, which was synthesized as following steps: "$W_5O_{18}{}^{6-}$" $\xrightarrow{Co^{2+}}$ $[\{CoW_5O_{18}H\}_2]^{6-}$ $\xrightarrow{pyridine}$ $[(py)CoW_5O_{18}H]^{3-}$. In this paper, we have calculated all possible electronic states for $[(py)CoW_5O_{18}]^{4-}$ (with 1 or 3 unpaired electrons for Co). For simplification, $[(py)CoW_5O_{18}]^{4-}$ is defined as CoW_5. The relative energy difference between the quadruplicity state ($^4CoW_5$) and doublet state ($^2CoW_5$) is 0.345 eV which was obtained by BP86 method. In order to confirm the ground state of CoW_5, different methods (PBE, PW91, and CAM-B3LYP) were also selected, and the relative energies are collected in Table 1. The results show that the high spin state is more stable than low spin state for CoW_5. Saito et. al has shown that the hybrid functional of B3PW91 or CASPT2 and the MkCCSD, which includes dynamic electron correlations could be more accurate to predict the singlet–triplet energy gap for orangic species [67, 68]. To analyze the effect of late transition metals, $[(py)Fe^{II}W_5O_{18}]^{4-}$ (simplify as FeW_5) and $[(py)Ni^{II}W_5O_{18}]^{4-}$ (simplify as NiW_5) were also studied. Three possible electronic configurations for FeW_5 were calculated, and the quintet state ($^5FeW_5$) is more stable than the triplet state ($^3FeW_5$) and singlet state ($^1FeW_5$) by 0.360 and 0.445 eV, respectively. As for NiW_5, the triplet state ($^3NiW_5$) is more stable than singlet state ($^1NiW_5$) by 2.058 eV. And the HOMO energy levels of high spin states are lower than those of low spin states (Fig. S1, Supporting Information). So the ground states of $[(py)M^{II}W_5O_{18}]^{4-}$ (M = Co, Fe, Ni) are high spin states. For the present spin-unrestricted calculations, the calculated square of total spin is quite close to its eigenvalues $s(s + 1)$, indicating that the spin contamination is minor (see Table S1, Supporting Information).

The selected optimized bond distances of FeW_5, CoW_5, and NiW_5 are shown in Table 2. The calculated bond lengths of Co–N, Co–O_b and Co–O_c, which were calculated by BP86 method with COSMO, are in good agreement with the experimental data, as the discrepancy in the bond lengths deviations between theory and experiment was always smaller than 0.1 Å [69]. In addition, Table S2 display the selected optimized bond distances of CoW_5 by BP86, PW91, PBE and CAM-B3LYP methods. It is noticeable that, the optimized bond distances of $^4CoW_5$ calculated by BP86 method are in accordance with experimental data. For $[(py)MW_5O_{18}]^{4-}$, the bond lengths of M–N decrease as M = Fe (2.033 Å) > Co (2.022 Å) > Ni (2.006 Å), and the M–O_c distances have the same trend, which relate to the size of the M atom. While for M–O_b, the bond lengths decrease as M = Ni ~ Fe > Co.

As the systems FeW_5 and NiW_5 have not been synthesized by experiment, we discussed all the possible spin states to take full consideration. In the case of FeW_5, the bond lengths of Fe–N slightly increase with the trend of $^1FeW_5 < {}^3FeW_5 < {}^5FeW_5$. The trend of bond lengths of Co–N and Ni–N are same with Fe–N. For M–O_b, the bond length of $^1FeW_5$ (1.980 Å) is shorter than those of $^3FeW_5$ (2.086 Å) and $^3FeW_5$ (2.078 Å). And the bond length of NiW_5 with low spin state is also shorter than that of high

Table 1 The relative energy (eV) for two spin states CoW_5 obtained by the BP86, PBE, PW91 and CAM-B3LYP methods

	BP86	PBE	PW91	CAM-B3LYP
$^2CoW_5$	0.345	0.362	0.319	0.656
$^4CoW_5$	0.0	0.0	0.0	0.0

Table 2 The selected bond lengths [Å] of FeW_5, CoW_5, and NiW_5 by BP86 method

Bond	M–N	M–O_b	M–O_c
$^1FeW_5$	1.852	1.980	2.036
$^3FeW_5$	1.868	2.086	2.006
$^5FeW_5$	2.033	2.078	2.289
$^2CoW_5$	2.009	1.966	2.265
$^4CoW_5$	2.022 (2.025)[a]	2.065 (2.052)	2.244 (2.262)
$^1NiW_5$	1.953	2.097	2.067
$^3NiW_5$	2.006	2.080	2.122

[a] The bond lengths in parentheses belongs to experiment values [20]

spin state. While the distances of M–O_b for $^2CoW_5$ and $^4CoW_5$ are 1.966 Å and 2.065 Å, which are different from FeW_5 and NiW_5. Moreover, as the M atoms states are different, the change of M–O_c distances is different. For FeW_5 and NiW_5, the M–O_c distances of high spin states are longer than those of low spin states. Conversely, the M–O_c distance of $^4CoW_5$ is shorter than that of $^2CoW_5$.

3.2 Bonding character

According to the previous work, the Mo≡N triple bond has been proposed on the basis of its short bond length and nearly linear Mo–N–C bond angle in arylimido-hexamolybdate [70]. And the strong Mo≡N bond in organoimido derivatives of hexamolybdates was also first proved by our group [28, 29] using DFT method. Herein, it is interesting to investigate the bonding character of M–N bond in $[(py)MW_5O_{18}]^{4-}$.

In order to investigate the bonding feature between the M (M = Fe, Co, Ni) and N centers in the present species, the extent of bonding interaction between the M and N centers in the $[(py)MW_5O_{18}]^{4-}$ anions were calculated by using NBO theory. Herein we select the most stable spin states for investigating. The conventional parameters are used to characterize the bonding situation in molecules: the bond orders and NBO distribution have been analyzed in this work. For visualizing the M–N bond, some relevant orbitals of anions FeW_5, CoW_5, and NiW_5 were listed.

The calculated orbital hybridization and orbital type are shown in Table 3. NBO analysis reveals that $^5FeW_5$ has one Fe–N σ-bond composed of a $sp^{2.48}d^{1.45}$ Fe and a $sp^{2.27}$ N, and a Fe–N π-bond composed of a $sp^{1.00}d^{2.88}$ and one pure N p-orbital, respectively. From Fig. 3, it also can be found that FeW_5 have an σ-bond orbital and a π-bond orbital. For σ-bond scheme, the d_z^2-orbital of substituted iron atom gives the large contributions (50.50%). And the π-bond orbital of FeW_5 displays the large iron d-orbital composition (>60%). While for $^4CoW_5$ and $^3NiW_5$, there are one M–N σ-bond and three center bond (3c bond). And the relevant orbitals of $^4CoW_5$ and $^3NiW_5$ show the same result. The σ-bonds of Co–N and Ni–N contain 55.73% Co d_z^2-orbital and 48.38% Ni d_z^2-orbital, respectively. But why does the bond of Fe–N possesses an σ-bond and a π-bond, and the bonds of Co–N and Ni–N have only σ-bond? It proposes that the C–N bond in $^5FeW_5$ has only one σ-bond composed of one $sp^{2.36}$ C and one $sp^{1.88}$ N. While for $^4CoW_5$ and $^3NiW_5$, 3c bond are formed by two carbon atoms and one nitrogen atom. Moreover, the Wiberg bond indices (WBI) of M–N for three compounds increase as follows: $^5FeW_5$ (0.354) > $^4CoW_5$ (0.300) > $^3NiW_5$ (0.231), which indicates the interactions between metal M and N in these systems are all weak. For pyridine ligand,

Table 3 The analysis of NBO for $[(py)MW_5O_{18}]^{4-}$ anions

Compound	Bond	Occupancy	Orbital hybridization	Orbital type
$^5FeW_5$	Fe–N	0.966	$0.946sp^{2.27}$(N) + $0.323sp^{2.48}d^{1.45}$(Fe)	σ
		0.885	$0.843p$(N) + $0.538sp^{1.00}d^{2.88}$(Fe)	π
	Fe–O_b	0.895	$0.944p$(O) + $0.338sp^{1.84}d^{3.08}$(Fe)	σ
	C–N	0.991	$0.627sp^{2.36}$(C) + $0.779sp^{1.88}$(N)	σ
$^4CoW_5$	Co–N	0.967	$0.954sp^{2.19}$(N) + $0.299sp^{3.36}d^{2.31}$(Co)	σ
	Co–O_b	0.889	$0.941p$(O) + $0.339sp^{0.37}d^{1.09}$(Co)	σ
	C–N	0.991	$0.630sp^{2.32}$(C) + $0.777sp^{1.91}$(N)	σ
	C–C-N	0.967	$0.463p$(C) + $0.463p$(C) + $0.756p$(N)	π
$^3NiW_5$	Ni–N	0.967	$0.955sp^{2.28}$(N) + $0.296sp^{3.75}d^{2.08}$(Ni)	σ
	Ni–O_b	0.880	$0.978sp^{0.77}$(O) + $0.207sp^{3.03}d^{1.90}$(Ni)	σ
	C–N	0.991	$0.629sp^{2.33}$(C) + $0.778sp^{1.88}$(N)	σ
	C–C–N	0.972	$0.458p$(C) + $0.458p$(C) + $0.762p$(N)	π

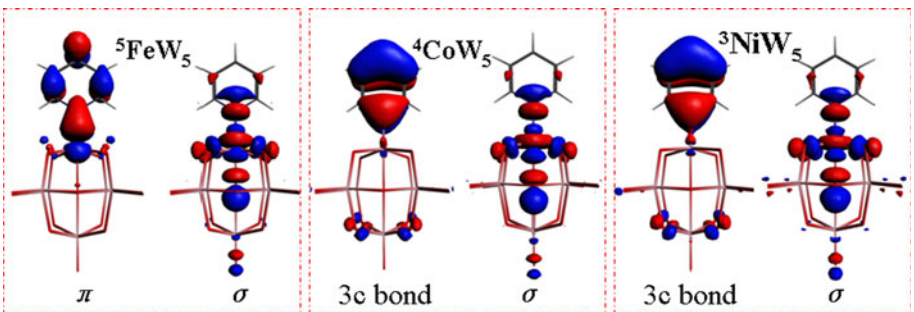

Fig. 3 Plot of some relevant orbitals of anions $^5FeW_5$, $^4CoW_5$, and $^3NiW_5$ showing visualization of the M–N (M = Fe, Co, Ni) bonding

interactions between carbon atoms and nitrogen atom are strong. The WBI of C–N for $^5FeW_5$, $^4CoW_5$ and $^3NiW_5$ are 1.253, 1.337 and 1.369, respectively. It is well known that the molecular orbital was combined by atomic orbitals according to three fundamental principles: (1) similar energies of two atomic orbitals; (2) maximum overlap between two atomic orbitals; (3) adapted symmetry. From the DFT calculation results, it is found that the principle of similar energies is important for forming M–N π-bonds in $^5FeW_5$, $^4CoW_5$ and $^3NiW_5$ as the M–N π-bonds are composed of M d_{xz}-orbital and N p_z-orbital. The absolute energy gaps between M d_{xz}-orbital and N p_z-orbital for $^5FeW_5$, $^4CoW_5$ and $^3NiW_5$ are 0.395, 1.110, and 2.969 eV, respectively. So the Fe d_{xz}-orbital and N p_z-orbital prefer to form Fe–N π-bond. While it is difficult to form M–N π-bond for $^4CoW_5$ and $^3NiW_5$ as the energy gaps between M d_{xz}-orbital and N p_z-orbital are larger.

3.3 Orbital character

It is well known that the occupied orbitals of $[W_6O_{19}]^{2-}$ formally delocalize over the bridge oxygen atoms and slightly on tungsten atoms, and the unoccupied orbital are symmetry adapted *d*-metal orbitals with some antibonding participation of oxygen *p*-orbitals [71]. We continue to investigate the influence of the substituted transition metal and pyridine on the electronic properties of $[(py)MW_5O_{18}]^{4-}$. The ground states of FeW_5, CoW_5, and NiW_5 were chosen to discuss. The frontier molecular orbitals (FMOs) of $[(py)MW_5O_{18}]^{4-}$ are shown in Fig. 4. The highest single occupied molecular orbital (β-HOMO) in system $^5FeW_5$ delocalizes over the iron atom (64.58%) and slightly on pyridine (12.14% in carbon atoms which connect with nitrogen atom and 10.82% in other two carbon atoms). The β-HOMO of $^4CoW_5$ delocalizes over the substituted transition Co metal (89.73%). While the β-HOMO in $^3NiW_5$ is contributed among *d*-Ni orbital (44.87%), O_c and O_b *p*-orbital (17.16% and 16.56%) with slight component of *p*-N orbital (9.47%). It suggests that the substituted transition metal atoms affect the β-HOMOs of $[(py)MW_5O_{18}]^{4-}$ anions. The lowest unoccupied molecular orbitals (β-LUMOs) of three systems mainly delocalize over the substituted transition metal atoms and some participation of bridge oxygen which links to the substituted transition metal atoms. While the β-LUMO + 1 mainly delocalize over the pyridine. It indicates that the substituted transition metal plays an important role in the FMOs.

There is no doubt that the redox properties of the substituted clusters depend on the energies and compositions of the β-LUMOs. Lower β-LUMO energy means that the cluster is more easily reduced [30]. It is well known that tungsten atom is substituted by a higher electronegative atom, such as Mo and V etc., the redox properties of the substituted systems would be remarkably changed [72]. The β-LUMO energies of systems $^5FeW_5$, $^4CoW_5$ and $^3NiW_5$ are −0.22, −0.68 and −0.07 eV, respectively. The β-LUMO energy of system $^4CoW_5$ is lower than those of $^5FeW_5$ and $^3NiW_5$. So system CoW_5 is more easily reduced in three systems. According to the molecular orbital diagram in Fig. 4, the substituted transition metal atoms (Fe, Co and Ni) prefer to accept an extra electron when the cluster is reduced.

The total density of states (TDOS) and projected density of states (PDOS) are helpful for analyzing the electronic structures of molecules. In this respect, TDOS and PDOS calculated for $^5FeW_5$, $^4CoW_5$ and $^3NiW_5$ are presented in Fig. 5. It reveals that the carbon, oxygen and tungsten atoms play the significant roles in the formation of α-LUMOs for three systems, while for the α-HOMOs originates mainly from oxygen and M (M = Fe, Co, and Ni) atoms. For β-molecular orbitals of $^5FeW_5$ and $^4CoW_5$, the substituted transition metal atoms (Fe and Co) play important role in the formation of β-LUMOs and β-HOMOs around the β-HOMO-LUMO gap. However, the β-molecular orbitals of $^3NiW_5$ have a little different from $^5FeW_5$ and $^4CoW_5$. The nickel atom is little contributed to β-LUMOs and β-HOMOs around the β-HOMO-LUMO gap. In summary, Fe, Co, and Ni atoms mainly display electron donor character for $^5FeW_5$, $^4CoW_5$ and $^3NiW_5$, respectively.

3.4 Second-order polarizabilities

POMs are excellent electron accepter and can form electron donor–acceptor compounds. Experimental and theoretical investigations have shown that the POM-based hybrid complexes hold remarkably large NLO response [73–77].

The first hyperpolarizabilities of all systems considered in this study were calculated under the static electronic field. The total second-order polarizabilities β_0 for the studied compounds are defined in the following equation:

$$\beta_0 = \left(\beta_x^2 + \beta_y^2 + \beta_z^2\right)^{\frac{1}{2}}, \tag{2}$$

where β_x, β_y and β_z are the components of the second-order polarizability tensor along the x-, y- and z-axes, respectively. The vector component of β (β_i) is defined by the equation shown below:

$$\beta_i = \beta_{iii} + \frac{1}{3}\sum_{j\neq i}\left(\beta_{ijj} + \beta_{jij} + \beta_{jji}\right). \tag{3}$$

Herein, β_{iii} is the diagonal tensor. For a chromophore with C_{2v} symmetry, there are five nonzero components of the β tensor, β_{zzz}, β_{zyy}, β_{zxx}, β_{yyz} and β_{xxz}. Assuming Kleinman

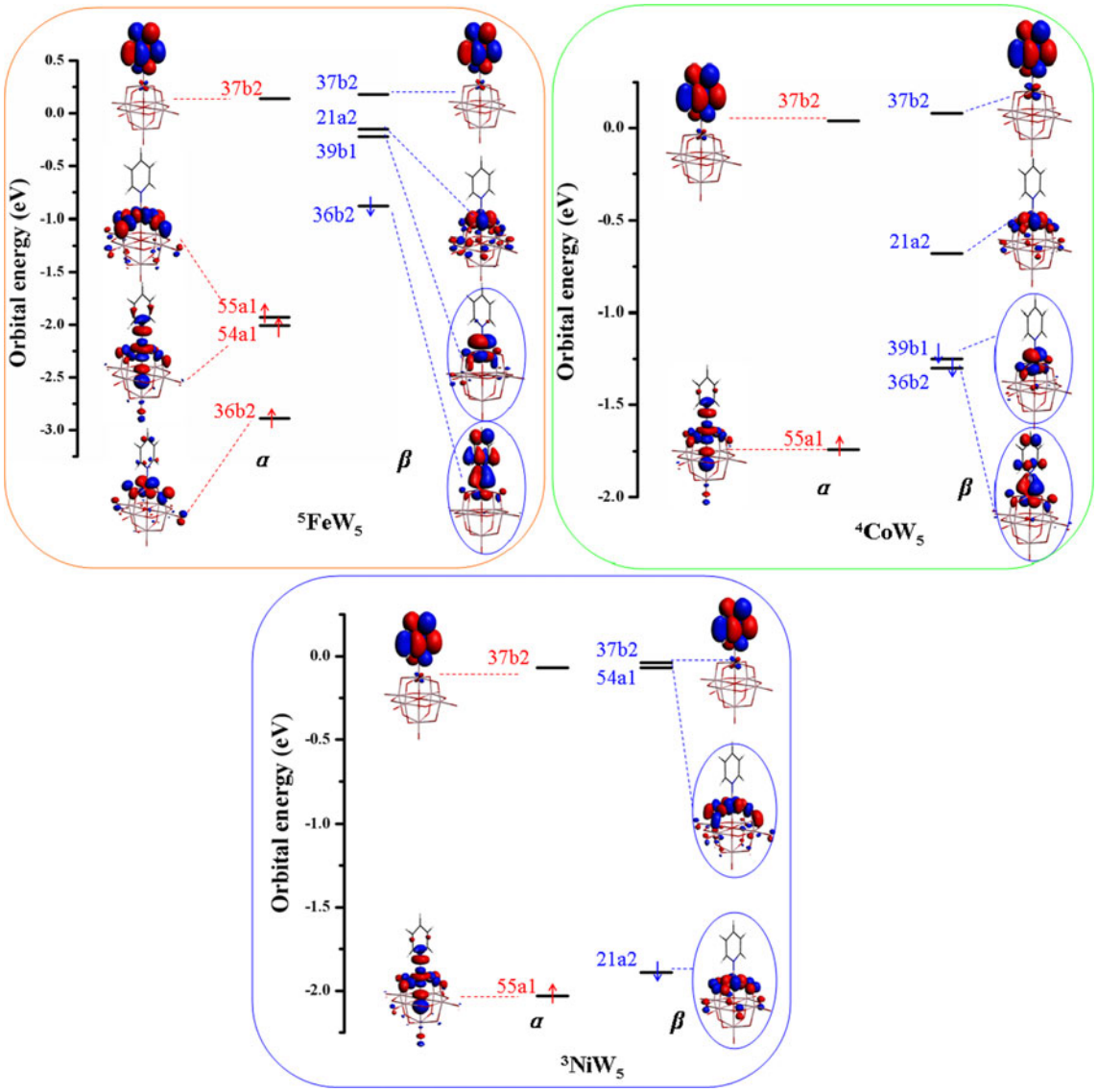

Fig. 4 The orbital energy and frontier molecular orbital of $^5FeW_5$, $^4CoW_5$ and $^3NiW_5$

symmetry, $\beta_{zyy} = \beta_{yyz}$ and $\beta_{zxx} = \beta_{xxz}$. The total β_0 and the corresponding β_{zzz}, β_{zxx}, and β_{zyy} tensor components are shown in Table 4. The computed β_0 values of three systems increase as following order: $^5FeW_5 > {}^4CoW_5 > {}^3NiW_5$. The β_{zzz} values also increase according to this order. It is further confirmed that the main contribution of β_0 is in z-axis. The results indicate that the high spin state in FeW_5 exhibit significant NLO response (525.103×10^{-30} esu), which is 4.5 and 17.5 times larger than those of $^4CoW_5$ and $^3NiW_5$. It proposes that the strong interaction in $^5FeW_5$ generates a strong electronic communication between pyridine and iron atom. The first hyperpolarizabilities of same polyanion with different spin configurations were also calculated. From Table 4, it can be found that the calculated β_0 values of different electronic states for FeW_5 show the following order: $^5FeW_5 > {}^3FeW_5 > {}^1FeW_5$. That is, the β_0 values of $^5FeW_5$ is about 2 times larger than that of $^3FeW_5$, and 4 times larger than that of $^1FeW_5$. The β_0 values of CoW_5 and NiW_5 with different electronic states are similar. In other words, the high spin state in system FeW_5 presents considerable large β_0 value, which is larger than those of triplet state and singlet state. While in CoW_5 and NiW_5, different electronic states do not affect the β_0 values.

In order to elucidate the origin of nonlinear second-order responsibilities of these complexes, the two-level model is a simple link between hyperpolarizability and its electronic transistion in low-lying excited states. The static first hyperpolarizability is expressed by the following expression

$$\beta \propto \frac{\Delta\mu_{eg} f_{eg}}{E_{ge}^3}, \tag{4}$$

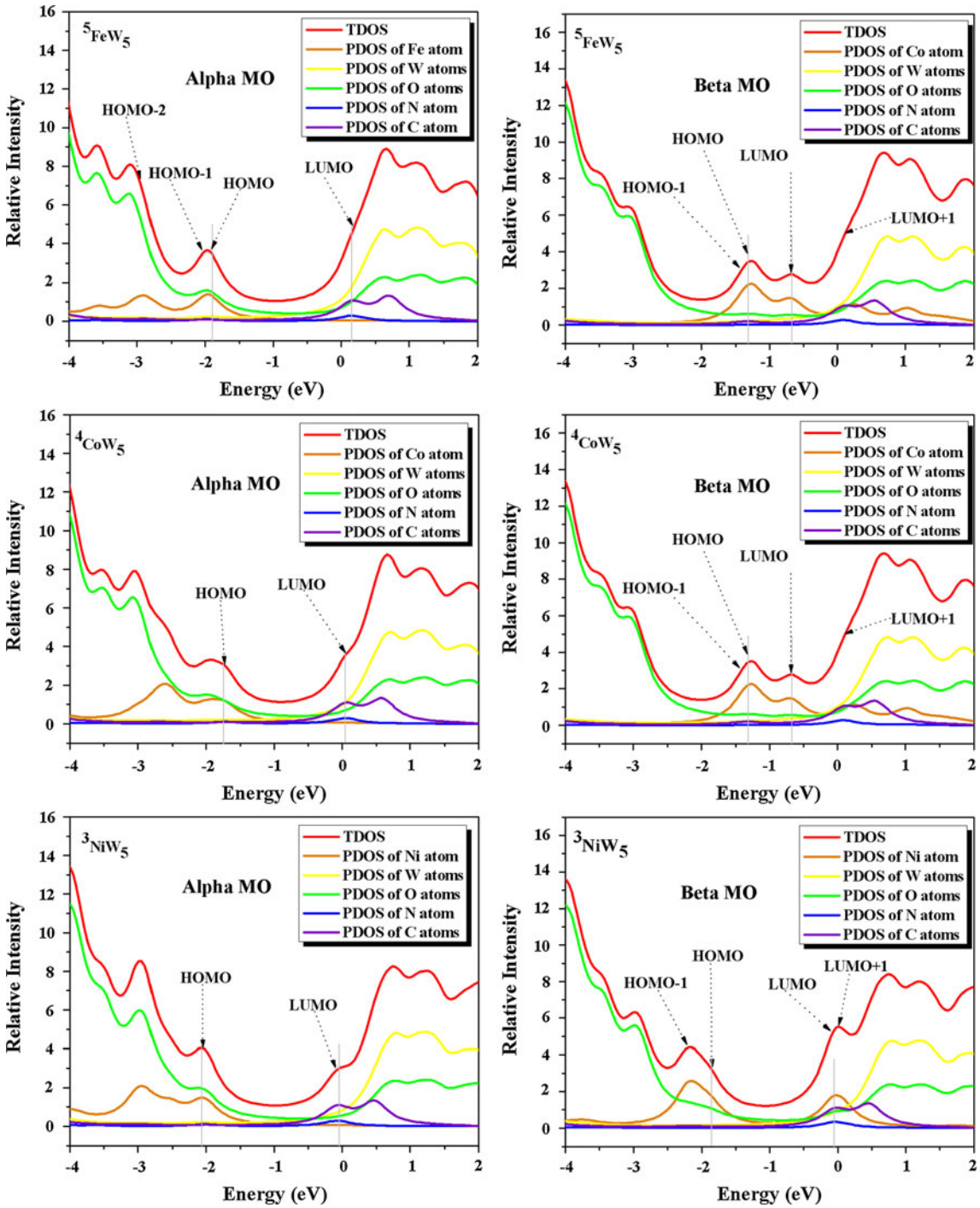

Fig. 5 Total and partial density of states (TDOS and PDOS) around the HOMO–LUMO gap for $^5FeW_5$, $^4CoW_5$ and $^3NiW_5$

where $\Delta\mu_{eg} = \Delta\mu_e - \Delta\mu_g$ is the change of dipole moment between the ground state and excited state, E_{ge} is the transition energy and f_{eg} is the oscillator strength. The first hyperpolarizability is jointly determined by $\Delta\mu_{eg}$, f_{eg}, and E_{ge} quantities. Therefore, the first hyperpolarizabilities for three systems are mainly proportional to f_{eg} and inversely proportional to the cube of E_{ge}. The transition energy (E_{ge}) and oscillator strength (f_{eg}) are listed in Table 5. The results show that the transition energies for $^5FeW_5$, $^4CoW_5$ and $^3NiW_5$ are 1.902, 2.380, and 3.195 eV, respectively. In addition, the oscillator strength of system $^5FeW_5$ is 2 times larger than that of $^4CoW_5$, and 4 times larger than that of $^3NiW_5$. According to the two-level formula, the first hyperpolarizability for system $^5FeW_5$ is larger than those of

Table 4 The total second-order polarizability β_0 ($\times 10^{-30}$ esu) values for the compounds

	FeW_5			CoW_5		NiW_5	
	$^1FeW_5$	$^3FeW_5$	$^5FeW_5$	$^2CoW_5$	$^4CoW_5$	$^1NiW_5$	$^3NiW_5$
β_{zzz}	61.46	262.51	525.10	118.68	120.72	34.78	30.45
β_{zxx}	1.14	4.92	5.21	0.80	0.47	0.81	0.83
β_{zyy}	−0.45	−3.56	−0.11	1.79	0.97	3.09	0.91
β_0	62.15	263.87	530.21	121.27	122.15	38.68	32.18

Table 5 Oscillator strengths (f), excitation energy (E = eV), and corresponding dominant MO transitions of $[(py)MW_5O_{18}]^{4-}$ (M = Fe, Co, Ni)

Systems	Spin state	E_{ge}	f_{eg}	Major transition	
FeW_5	$^1FeW_5$	2.511	0.022	69b1 → 72b1	86.30%
	$^3FeW_5$	1.977	0.071	β 69b1 → β 70b1	82.56%
	$^5FeW_5$	1.902	0.140	β 69b1 → β 70b1	89.81%
CoW_5	$^2CoW_5$	2.088	0.026	β 69b1 → β 70b1	80.29%
	$^4CoW_5$	2.380	0.072	β 69b1 → β 70b1	97.05%
NiW_5	$^1NiW_5$	2.853	0.024	69b1 → 70b1	85.13%
	$^3NiW_5$	3.195	0.036	β 69b1 → β 70b1	95.44%

$^4CoW_5$ and $^3NiW_5$. The f_{eg}/E^3_{ge} values of system $^4CoW_5$ and $^3NiW_5$ are 0.005 and 0.001, respectively. That results in the relatively smaller β_0 value for $^3NiW_5$ than that of $^4CoW_5$.

The TDDFT calculations are also carried on different spin states for $[(py)M^{II}W_5O_{18}]^{4-}$ to analyze the origin of the NLO property. From Table 5 it is found that the transition energies of FeW_5 with different electronic states increase as following: $^5FeW_5$ (1.902 eV) < $^3FeW_5$ (1.977 eV) < $^1FeW_5$ (2.511 eV), while the oscillator strengths decrease from $^5FeW_5$ to $^1FeW_5$. So the first hyperpolarizabilities of FeW_5 are increased from $^5FeW_5$, $^3FeW_5$ to $^1FeW_5$. While for CoW_5 and NiW_5 with different spin states, the transition energy increase from low spin state to high spin state, and the oscillator strengths have the same changing trend. Therefore, the first hyperpolarizabilities of CoW_5 and NiW_5 do not change with the spin configurations changing.

In our previous study, the main origin of the NLO properties of organoimido derivatives of hexamolybdates is the charge transfer from organoimido to polyanion [28, 29]. The compounds $[(py)MW_5O_{18}]^{4-}$, which may exhibit a metal-to-ligand charge transfer (MLCT) that was based on major electron transitions orbitals analysis. The molecular diagrams involving the orbital transition of system FeW_5 with three spin states are displayed in Fig. 6. In system $^1FeW_5$, the transition can be assigned to the charge transfer from the iron atoms to tungsten and oxygen atoms. For systems $^3FeW_5$ and $^5FeW_5$, the pyridine becomes an acceptor and the Fe act as donors. The charge transfer of systems CoW_5 and NiW_5 with different spin states are similar to that of $^3FeW_5$ and $^5FeW_5$ (See Fig. S2).

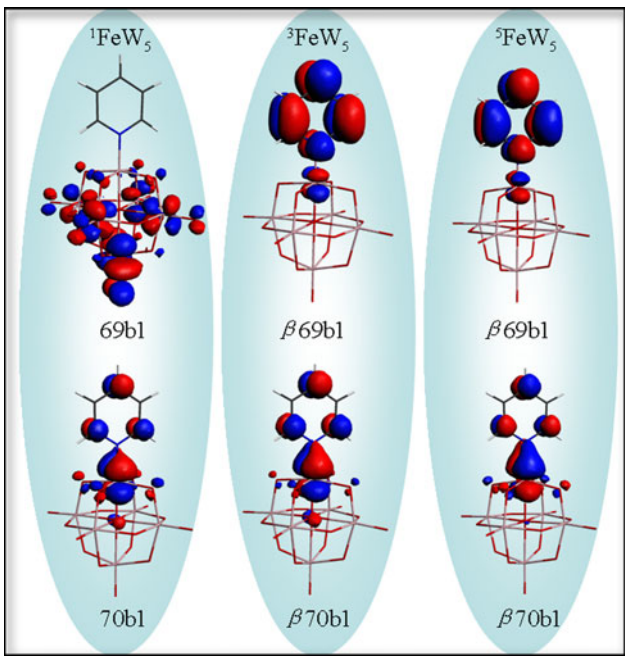

Fig. 6 The major electron transitions orbitals of FeW_5

It is quite obvious that the effect of substituted metals has significant influence on the second-order NLO property of $[(py)MW_5O_{18}]^{4-}$. And different spin configurations also affect the second-order NLO property of $[(py)MW_5O_{18}]^{4-}$.

4 Conclusions

In this paper, we have performed systematic DFT calculations of geometrical structures, NBO analysis, electronic

properties, and second-order NLO properties of substituted Lindqvist-type POMs containing late 3d transition metals, $[(py)MW_5O_{18}]^{4-}$ (M = Fe, Co, Ni). (1) The results show that the bond lengths of M–N decrease as M = Fe > Co > Ni, and the same trend for M–O_c. (2) The NBO analysis shows that $[(py)MW_5O_{18}]^{4-}$ possesses weak M–N bonding, which is different from the Mo≡N bond as showed in $[Mo_6O_{18}NPh]^{2-}$. (3) The FMOs of $[(py)MW_5O_{18}]^{4-}$ (M = Fe, Co, Ni) show new characters comparing with $[W_6O_{19}]^{2-}$. The β-HOMOs of $[(py)MW_5O_{18}]^{4-}$ delocalize over the substituted metal atoms, while the β-LUMOs mainly localizes on the substituted transition metal atoms and bridge oxygen which links to the substituted transition metal atom M. Additionally, the β-LUMO + 1 mainly delocalize over the pyridine. (4) TDDFT calculations suggest that the charge transfer mainly from the substituted transition metals to the pyridine segment along the z-axis plays the key role in the NLO response of $[(py)MW_5O_{18}]^{4-}$. This is the different case compared with the organoimido derivatives of hexamolybdates which show opposite charge transfer phenomena. The computed β_0 values of three systems increase as following order: $^3NiW_5 < {}^4CoW_5 < {}^5FeW_5$. And with different spin configurations, the β_0 value of system $^5FeW_5$ is larger than those of $^3FeW_5$ and $^1FeW_5$. While for CoW_5 and NiW_5, the spin configurations do not affect their β_0 values.

Acknowledgments The authors gratefully acknowledge financial support from NSFC (20971020 and 21073030), PCSIRT (IRT-0714), and the Science and Technology Development Planning of Jilin Province (20100104). We also acknowledge Yu He Kan for computational support.

References

1. Pope MT (1983) Heteropolyand IsopolyOxometalates [M]. Springer, Heidelberg
2. Muller A, Peters F, Pope MT et al (1998) Chem Rev 98:239
3. Wang C, Ren Y, Du C et al (2010) Cryst Eng Comm 12:3522
4. Mizuno N, Misono M (1998) Chem Rev 98:199
5. Pope MT, Müller A (1991) Angew Chem Int Ed Engl 30:34
6. Yan J, Long DL, Cronin L (2010) Angew Chem Int Ed 49:1
7. Elena A, Christian N, Paul K et al (2011) Angew Chem Int Ed 50:764
8. Gouzerh P, Proust A (1998) Chem Rev 98:77
9. Dablemont C, Proust A, Thouvenot R et al (2004) Inorg Chem 43:3514
10. Duhacek JC, Duncan DC (2007) Inorg Chem 46:7253
11. Proust A, Thouvenot R, Gouzerh P (2008) Chem Commun 16:1837
12. Hao J, Xia Y, Wang L et al (2008) Angew Chem Int Ed 47:2626
13. Xu B, Lu M, Kang J et al (2005) Chem Mater 17:2841
14. Chen G, Ma P, Wang J et al (2010) J Coord Chem 63:3753
15. Xu H, Li Z, Liu B et al (2010) Cryst Growth Des 10:1096
16. Che TM, Day VW, Francesconi LC et al (1985) Inorg Chem 24:4055
17. Che TM, Day VW, Francesconi LC et al (1992) Inorg Chem 31:2920
18. Taban-Çalışkan G, Agustin D, Demirhan F et al (2009) Eur J Inorg Chem 2009:5219
19. Klemperer WG, Main DJ (1990) Inorg Chem 29:2355
20. Errington RJ, Harle G, Clegg W et al (2009) Eur J Inorg Chem 2009:5240
21. Da Silva A, Junqueira G, Anconi C et al (2009) J Phys Chem C 113:10079
22. Blau W (1987) Phys Tech 18:250
23. Bredas JL, Adant C, Tackx P et al (1994) Chem Rev 94:243
24. Powell CE, Humphrey MG (2004) Coord Chem Rev 248:725
25. Attanasio D, Bonamico M, Fares V et al (1990) J Chem Soc 11:3221
26. Williamson MM, Bouchard DA, Hill CL (1987) Inorg Chem 26:1436
27. Pope MT, Muller A (2001) Polyoxometalate Chemistry From Topology via Self Assembly to Applications. Springer, Verlag
28. Yan LK, Yang GC, Guan W et al (2005) J Phys Chem B 109:22332
29. Yang GC, Guan W, Yan LK et al (2006) J Phys Chem B 110:23092
30. López X, Bo C, Poblet JM (2002) J Am Chem Soc 124:12574
31. Liu CG, Su ZM, Guan W et al (2009) Inorg Chem 48:541
32. Yan LK, Su ZM, Guan W et al (2004) J Phys Chem B 108:17337
33. Te Velde G, Bickelhaupt FM, Baerends EJ et al (2001) J Comput Chem 22:931
34. Fonseca Guerra C, Snijders JG, te Velde G et al (1998) Theor Chem Acc 99:391
35. ADF2008.01:SCM, Vrije Universiteit: Amsterdam, The Netherlands. http://www.scm.com
36. Chang C, Pelissier M, Durand P (1986) Phys Scr 34:394
37. Lenthe Ev, Baerends EJ, Snijders JG (1993) J Chem Phys 99:4597
38. Lenthe Ev, Baerends EJ, Snijders JG (1994) J Chem Phys 101:9783
39. Van Lenthe E, Van Leeuwen R, Baerends EJ et al (1996) Int J Quantum Chem 57:281
40. Becke AD (1988) Phys Rev A 38:3098
41. Perdew JP (1986) Phys Rev B 33:8822
42. Vosko SH, Wilk L, Nusair M (1980) Can. J. Phys. 58:1200
43. Guan W, Liu CG, Song P et al (2009) Theor Chem Acc 122:265
44. Klamt A, Schuurmann G (1993) J Chem Soc, Perkin Trans 2:799
45. Klamt A (1995) J Phys Chem 99:2224
46. Klamt A, Jonas V (1996) J Chem Phys 105:9972
47. Pye CC, Ziegler T (1999) Theor Chem Acc 101:396
48. Hu SZ, Zhou ZH, Tsai KR (2003) Acta Phys Chim Sin 19:1073
49. Han WG, Jalkanen KJ, Elstner M et al (1998) J Phys Chem B 102:2587
50. Tajkhorshid E, Jalkanen KJ, Suhai S (1998) J Phys Chem B 102:5899
51. Frimand K, Jalkanen KJ, Bohr HG et al (2000) Chem Phys 255:165
52. Jalkanen KJ, Degtyarenko IM, Nieminen RM et al (2008) Theor Chem Acc 119:191
53. Poon CD, Samulski ET, Weise CF et al (2000) J Am Chem Soc 122:5642
54. Deplazes E, van Bronswijk W, Zhu F et al (2008) Theor Chem Acc 119:155
55. Onsager L (1936) J Am Chem Soc 58:1486
56. Tomasi J, Persico M (1994) Chem Rev 94:2027
57. Frisch MJ, Trucks GW, Schlegel HB et al (2009) Gaussian 09. Revision A.01. Gaussian, Inc., Wallingford CT
58. Yanai T, Tew DP, Handy NC (2004) Chem Phys Lett 393:51
59. Kobayashi R, Amos RD (2006) Chem Phys Lett 420:106
60. Glendening ED, Badenhoop JK, Reed AE et al (2001) Theoretical Chemistry Institute. University of Wisconsin, Madison

61. Li G, Jia G, Gao Q, Feng Z et al (2010) J Phys Chem C 115:972
62. Rajapakse GVN, Soldatova AV, Rodgers MAJ (2010) J Phys Chem B 114:14205
63. Miao TF, Li J, Liao SY et al (2010) Inorg Chim Acta 363:3880
64. Badaeva E, Albert VV, Kilina S et al (2010) Phys Chem Chem Phys 12:8902
65. Song P, Yan LK, Guan W et al (2010) J Mol Graph Model 29:13
66. Schipper PRT, Gritsenko OV, van Gisbergen SJA et al (2000) J Chem Phys 112:1344
67. Saito T, Nishihara S, Yamanaka S, Kitagawa Y, Kawakami T, Yamada S, Isobe H, Okumura M, Yamaguchi K (2011) Theor Chem Acc. doi:10.1007/s00214-011-0914-z
68. Saito T, Nishihara S, Yamanaka S, Kitagawa Y, Kawakami T, Yamada S, Isobe H, Okumura M, Yamaguchi K (2011) Theor Chem Acc. doi:10.1007/s00214-011-0941-9
69. Maestre JM, Lopez X, Bo C et al (2001) J Am Chem Soc 123:3749
70. Wei Y, Xu B, Barnes CL et al (2001) J Am Chem Soc 123:4083
71. Yang X, Waters T, Wang XB et al (2004) J Phys Chem A 108:10089
72. Guan W, Yan LK, Su ZM et al (2005) Inorg. Chem. 44:100
73. Niu JY, You XZ, Duan CY et al (1996) Inorg Chem 35:421
74. Guan W, Yang GC, Yan LK et al (2006) Inorg. Chem. 45:7864
75. Xu XX, You XZ, Huang XY (1995) Polyhedron 14:1815
76. Zhang XM, Shan BZ, Duan CY et al (1997) Chem Commun 12:1131
77. Murakami H, Kozeki T, Suzuki Y et al (2001) Appl Phys Lett 79:3564